ISSN 2230-7850 Impact Factor : 4.1625 (UIF) Volume - 6 | Issue - 5 | June - 2016

Indian Streams Research Journal

Leveraging Off-the-Shelf WiFi for Contactless Activity Monitoring

Dr. Rekha
Assistant professor in Electronics Government college (Autonomous)Kalaburagi

Abstract:
For personalised health aids, monitoring human actions like walking, falling, and jumping yields important information. Current options use a high-definition camera to record video data, require the user to carry or wear specific smart gadgets, or deploy specialised equipment to collect wireless data. For various reasons, including pain, privacy, and overheads, none of these alternatives are, nevertheless, extensively used. Thus, there is a need for an efficient way to offer safe, affordable, and non-intrusive human activity monitoring. In this work, we designed a contactless human activity tracking system that makes use of the channel state information (CSI) of the current WiFi signals that are widely used. In particular, we utilised a desktop computer outfitted with an Intel WiFi Link 5300 NIC as the receiver and a cheap commercial off-the-shelf (COTS) router as the transmitter.

Keywords: contactless; activity monitoring; RF signals; channel state information

Introduction

In the context of modern life, it is of significant value to conduct indoor human activity detection. First, it allows for the monitoring of an individual's body posture and gait in real- time, which is beneficial from the perspective of health management for the early discovery of and protection from diseases due to sedentary behavior and unhealthy posture, among other aspects. Furthermore, human activity detection can reveal abnormal behaviors in a timely manner and reduce the incidence of accidents such as falling down for the elderly or people with limited mobility. In addition, indoor human activity detection also promotes the development of home automation with more personalized and intelligent services through intelligently recognizing and analyzing the activity habits of users.

As early as 2005, Kushida et al. employed polysomnography (PSG) for monitoring of the physical health of the human body [1,2]. However, polysomnography requires the user to wear dozens of sensors

and, consequently, is inapplicable for long and continuous human activity detection due to the high cost and invasiveness of the device. To overcome these limitations, researchers have attempted to employ built-in motion sensors (e.g., magnetometer, accelerometer, and gyroscope) in smartphones [3–5], smartwatches [6–9], and/or wearable devices [10,11] to capture and record data reflecting changes in human movement, thus realizing long and continuous human activity detection. While these approaches are effective in reducing the cost of the device, they also require users to attach intrusive sensors to their body throughout the monitoring process, which poses unrealistic demands for groups such as the elderly, children, and others. Wang et al. proposed a solution to the intrusiveness problem in contact sensing methods through utilization of the built-in speakers and microphones of smart devices to send and receive sound signals, respectively, then analyzed and processed the collected audio data to obtain useful information about human activities [12–14]. However, audio-based sensing methods are not only susceptible to ambient noise but also raise privacy concerns. Meanwhile, extensive works have employed cameras to collect and record image/video data of human activities, then adopted methods based on computer vision to obtain information about human activities of interest [15–19]. Nevertheless, video-based sensing methods rely on light conditions and also pose privacy risks; furthermore, they cannot be applied in situations where the target is obscured by obstacles.

With the development and innovation of wireless communication, human activity sensing based on radio frequency signals has attracted extensive attention, as it protects the privacy of the users while realizing contactless sensing. Specifically, sensing methods based on radar signals enable contactless and high-accuracy monitoring of human activities such as respiration, heart rate, and gesture perception [20–26]. However, the methods mentioned above require specialized devices, and they are complicated to widely deploy due to high hardware costs and complexity of operation. Similarly, the Universal Software Radio Peripheral (USRP)-based sensing approach requires not only the deployment of specialized hardware devices but also the writing of complex hardware programs [27–29]. To address the limitations of a high hardware cost and operating difficulty, researchers have utilized RFID readers and tags as transceivers of wireless signals to realize contact- less human body activity monitoring [30–34]. However, RFID-based sensing approaches require deploying dozens or even hundreds of tags, which creates an extreme limitation in practical applications. Therefore, we sought a solution that is low-cost, contactless, and privacy-preserving, to provide long-term continuous human activity monitoring. We found that Channel State Information of the existing ubiquitous WiFi signals is a desirable candidate. The reason is that given the prevalence of WiFi infrastructures in office or home environments, it is possible to capture people's activities without their participation [35].

Therefore, our study directly utilized the physical-layer attributes (i.e., CSI) of existing ubiquitous WiFi signals to obtain environmental information that is relevant to human activities, allowing for the construction of a low-cost, contactless, and privacy-preserving indoor human activity monitoring system. Briefly, we deployed and built WiFi sensing devices to collect and record WiFi CSI data reflecting changes in human activities. Then, we constructed a combined filtering channel to remove the outliers and ambient noise mixed

in the raw CSI data, to obtain fine-grained WiFi CSI signals. The different center frequencies of different CSI subcarriers result in different sensitivities of different CSI subcarriers to the same target action. Consequently, we constructed a novel sensitivity metric and selected an optimal set of subcarriers (i.e., top-ten subcarriers) from 30 candidate CSI subcarriers based on this metric. Eventually, we categorized the segmented CSI signals using a lightweight machine learning algorithm to implement accurate walking, falling, and jumping measurements. Compared to existing approaches, the advantages of the method proposed in this study are threefold: first, monitoring target human activities with CSI data based on WiFi signals is non-intrusive for the human body and protects the privacy of users better; second, using the existing WiFi routers and personal computers as the transmitters and receivers directly has a low cost and enables easy deployment; third, the strong penetration of WiFi signals can detect human activities in non-line-of-sight scenarios.

In summary, this study makes the following main contributions:

We propose a method for achieving contactless human activity sensing by utilizing ubiquitous WiFi signals, which is non-intrusive, low-cost, and secure for the user.

We have designed a novel metric based on kurtosis and standard deviation to select an optimal subcarrier set that is sensitive to all target activities from the candidate 30 subcarriers.

- We have implemented our system prototype with a COTS router and a desktop computer and conducted extensive experiments with 10 people over a period of one month. The results indicate the accuracy and robustness of our system.

Preliminaries

1.1. Channel State Information

Channel state information (CSI) describes the transmission process of a WiFi signal from transmitter to receiver at a specific carrier frequency, involving the effects of distance, fading, and scattering on the WiFi signal propagation. For a WiFi sensing system, when the number of antennas of the WiFi receiver and transmitter are M_R and M_T, the WiFi reception signal can be represented as

$$\boldsymbol{R}_i = \boldsymbol{H}_i \boldsymbol{S}_i + \boldsymbol{N}_i \quad (1)$$

where i is the index of the OFDM subcarrier, $\boldsymbol{S}_i \in R^{M_T}$ is the WiFi transmitting signal, $\boldsymbol{R}_i \in R^{M_R}$ is the WiFi reception signal, N_i is the noise vector, and $\boldsymbol{H}_i \in C^{M_R \times M_T}$ is expressed as the CSI matrix of the OFDM subcarrier i; that is,

$$\boldsymbol{H}_i = \begin{bmatrix} h_i^{11} & h_i^{12} & \cdots & h_i^{1M_T} \\ h_i^{21} & h_i^{22} & \cdots & h_i^{2M} \\ \vdots & \vdots & \ddots & \vdots \\ h_i^{M_R 1} & h_i^{M_R 2} & \cdots & h_i^{M_R M_T} \end{bmatrix} \quad (2)$$

where h_i^{rt} is denoted as the CSI value of the ith OFDM subcarrier in the communication link formed by receiving antenna r and transmitting antenna t, and h_i is a complex number, which can be further represented as

$$h_i^{rt} = I_i^{rt} + JQ_i^{rt} = \left\| h_i^{rt} \right\| e^{j\angle h_i^{rt}} \quad (3)$$

where Q_i^{rt} and I_i^{rt} are the quadrature component and in-phase component; and $\left\| h_i^{rt} \right\|$ and $\angle h_i^{rt}$

$_i$ are the amplitude and phase response of the subcarrier i, respectively. We can use open-source testing tools to extract CSI data from the wireless card of a WiFi receiver [36].

The multipath propagation schematic of a WiFi signal in a human activity scenario is shown in Figure 1. Specifically, the WiFi signal received at the WiFi receiver is a combinationof signals from different paths due to the multipath propagation effect of the WiFi signal,namely, the line-of-sight (LOS) path, the reflected path of a static object (i.e., the static path), and the reflected path of a human body's activity (i.e., the dynamic path). Hence, the CSI measurements extracted from the WiFi receiver are affected by factors such as the transceiver position, static object reflection, and dynamic human activity. Note that, when the transceiver location and the experimental scenario are determined, the static propagation path (i.e., the green solid line) in Figure 1 will remain relatively stable and, at this time, the changes in the CSI measurements will mainly depend on the changes in thedynamic propagation path (i.e., the red dashed line). That is to say, the CSI can be used torealize human activity monitoring by sensing dynamic propagation path changes in the multipath propagation of WiFi signals.

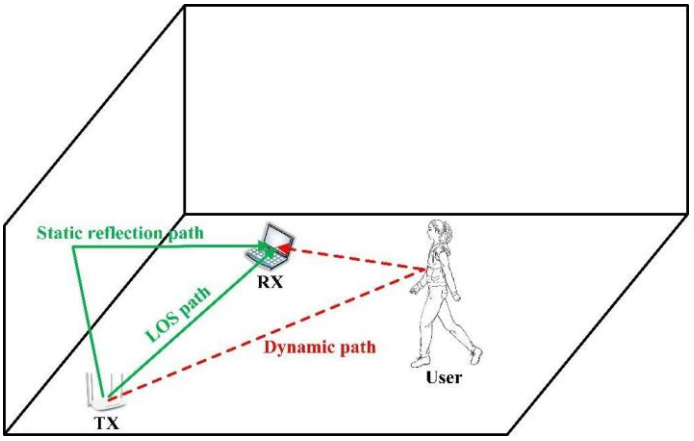

Figure 1. Illustration of WiFi signal multipath propagation.

1.2. *Support Vector Machine*

SVM is a powerful machine learning algorithm capable of processing data in high- dimensional spaces and realizing classification and regression analysis by finding optimal hyperplanes. It has achieved a wide range of applications in many fields such as image recognition, text classification and signal processing. The core idea is to find an optimal hyperplane that separates sample points of different categories as much as possible and maximizes the gap between the two categories. The overview diagram of the algorithm is shown in Figure 2.

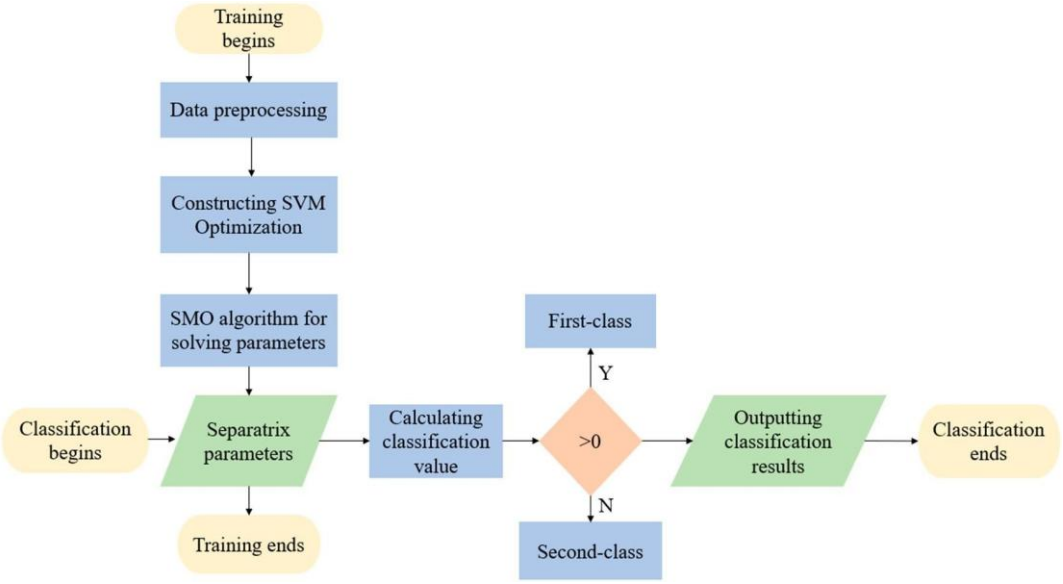

Figure 2. Overview diagram of the SVM algorithm.

2. System Design

2.1. System Overview

This study aimed to utilize the RF signals generated by a commercial WiFi routerto achieve device-free indoor human activity detection, which does not require the users to equip any sensing device. As illustrated in Figure 3, the proposed system first uses a commercial WiFi router as a transmitter to generate RF signals, while using a desktop computer as a receiver to receive RF signals and collect WiFi CSI data that record changes in human activities. As the raw CSI data contain a certain quantity of outliers and ambient noise, in the data processing module, we first constructed a combined filtering channel, comprising Hampel, wavelet, and moving average filters, in order to filter out the outliers and the ambient noise to obtain fine-grained CSI signals recording the changes in human activities. As different subcarriers have different center frequencies, this leads to different sensitivities of different subcarriers to the same target action. For this reason, we proposea new sensitivity metric, based on which we selected an optimal set of subcarriers from 30 candidate subcarriers, where any subcarrier within the optimal set can better record the CSI signal changes caused by the target action. In the motion recognition module, we performed reasonable segmentation of the selected optimal subcarriers to obtain CSI data segments recording different target actions, then extracted a set of feature sets containing both time- and frequency-domain features. Finally, we used the SVM algorithm to train a classification model to achieve accurate recognition of three human activities: walking,jumping, and falling.

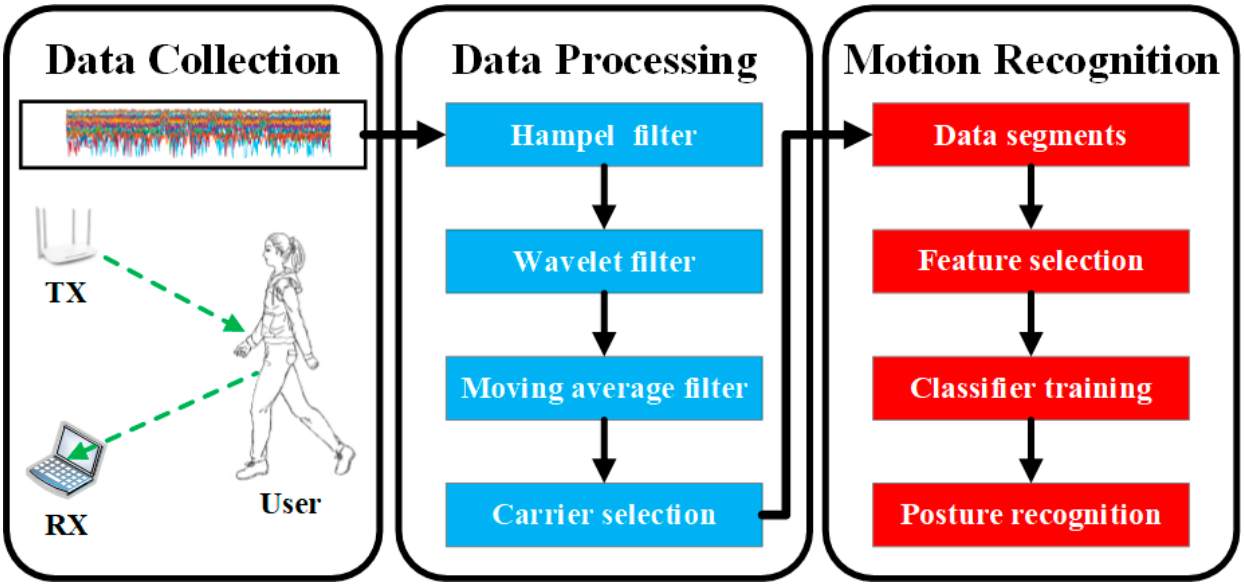

Figure 3. Proposed system architecture.

2.2. Data Collection

As shown in Figure 4, we deployed an indoor human activity sensing system based on WiFi signals in an office with an area of about 20 m^2 (width and length of about 4 m and 5 m, respectively). The WiFi transmitter and receiver were a commercial router and a Lenovo desktop computer, respectively. Moreover, in order to enhance the strength of the received signal, we gave the NIC three external antennas with a gain of 6 dBi. The heightof the transmitter and receiver from the ground was about 0.75 m, and the relative distance between them was about 2 m. We set the transmitter packet rate to 20 pkts/s. During the experiment, we asked volunteers to randomly perform the target human activities (i.e., walking, jumping, and falling) on a foam mat. We applied a tool provided in the literature [36] to obtain CSI measurements for 30 subcarriers from the NIC. At the sametime, we used the HD surveillance device already installed in the office to capture video data recording indoor human activities to obtain the ground truth and label the dataset.

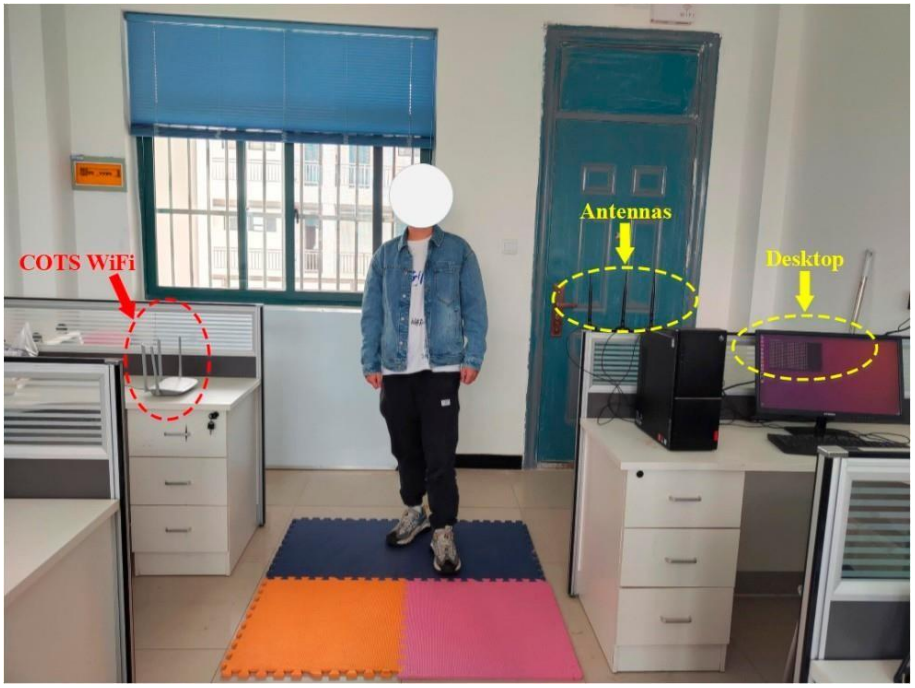

Figure 4. Deployment of the proposed system in an office.

2.3. *Data Processing*

The raw CSI measurements include a large number of outliers and ambient noise, which can seriously affect the perception of the system. Therefore, in order to extract effective features to raise the classification accuracy of the system, we needed to filter out the outliers and ambient noise mixed with the raw CSI data.

2.3.1. Hampel Filter

First of all, we filtered out the outliers mixed with the raw CSI data. Figure 5 depicts the amplitude variation in 30 unprocessed CSI subcarriers with human activities over a 30 s detection period. We can clearly observe that there are abnormal amplitudes in the CSI subcarriers at around 1 s, 6 s, 20 s, and 26 s. We filtered out these outliers utilizing the Hampel filter, which is a median and median absolute deviation (MAD)-based filter designed to identify and remove outliers in time-series data. The Hampel filter is more robust to outliers than traditional mean and standard deviation methods. Briefly, given

kth sliding window W_k^i = the CSI amplitude sequence $\{c_k^i, \ldots, c_{k+\Phi-1}^i\}$ $(1 \le k \le n - \Phi + 1)$ of length Φ if any CSI amplitude $c_j^i (k \le j \le k + \Phi - 1)$ within the current sliding window does not satisfy the condition $\mu_k^i - \gamma \times \sigma_k^i \le c_j^i \le u_k^i + \gamma \times \sigma_k^i$, then the Hampel filter treats it as an outlier. Here, μ_k^i and σ_k^i denote the median and MAD of the CSI amplitude in the current sliding window W_k^i, respectively, and γ is a variable constant. For any outlier c_j^i, the Hampel filter will replace it with the median value μ_k^i. Figure 6 shows the CSI amplitude variation after applying the Hampel filter to all 30 subcarriers. We can clearly observe that all the labeled outliers in Figure 5 were accurately removed. The result demonstrates that the Hampel filter is helpful for removing outliers from CSI data.

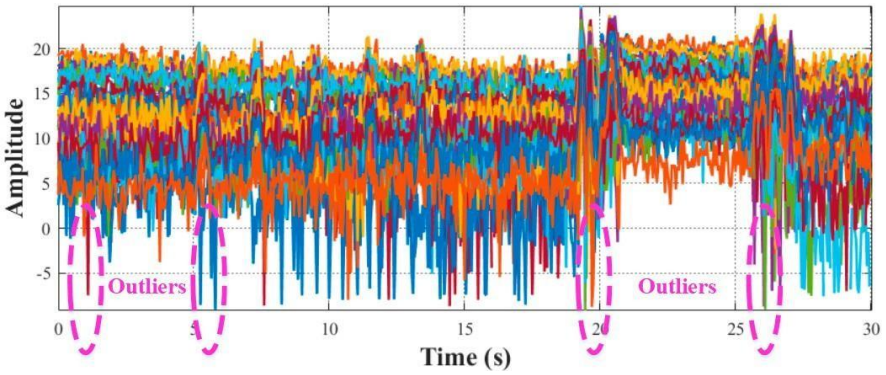

Figure 5. Raw CSI signals.

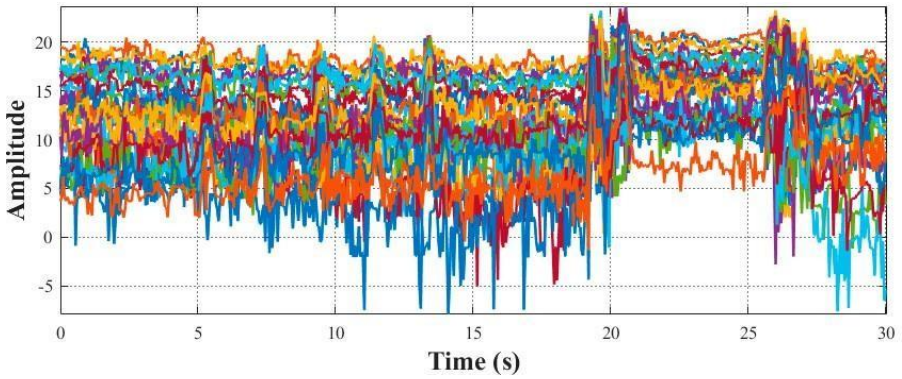

Figure 6. Hampel-filtered CSI signals.

2.3.2. Wavelet Filter

After removing outliers from the CSI data, we needed to further eliminate high- frequency ambient noise. Considering that human activities usually cause abrupt changes in the CSI amplitude, we thus needed to eliminate the high-frequency noise while also preserving the amplitude jumps in the CSI signal caused by human actions (i.e., the rising/falling edges in the CSI signal). In this context, conventional low-pass filters such as Butterworth filters and Chebyshev filters are no longer suitable, as they suppress not only high-frequency noise but also the rising/falling edges of the CSI signal. As wavelet filtering can effectively extract the transient and non-smooth information in the signal, itcan better deal with the abrupt changes and jumps in the signal. Therefore, we utilized the wavelet filter to eliminate the high-frequency noise and retain the rising/falling edges. Briefly, wavelet filtering achieves multi-scale decomposition and reconstruction of signals through the selection of appropriate wavelet basis functions and scale parameters. Common wavelet basis functions are Haar, Daubechies, Symlet, etc., which have different frequency characteristics and support ranges. The level decomposition and reconstruction equations for wavelet filtering are

$$x(t) = \sum_{j=0}^{J-1} \sum_{k} W_{j,k} \cdot \varphi_{j,k}(t) \tag{4}$$

where J represents the levels of decomposition, and $W_{j,k}$ is the jth level and kth wavelet coefficient. For data processing, we chose to use a 4-level 'db4' as the discrete wavelet basis function, Stein's unbiased estimation as the thresholding criterion, and soft thresholding, and only used the approximation coefficients to 'reconstruct' the filtered signal. Figure 7shows the CSI signals after wavelet filtering. Compared to Figure 6, we can clearly observethat this eliminated the high-frequency noise while also retaining the rising/falling edges in the CSI signal caused by human actions. The results indicate that the wavelet filter is useful for removing high-frequency noise from CSI data.

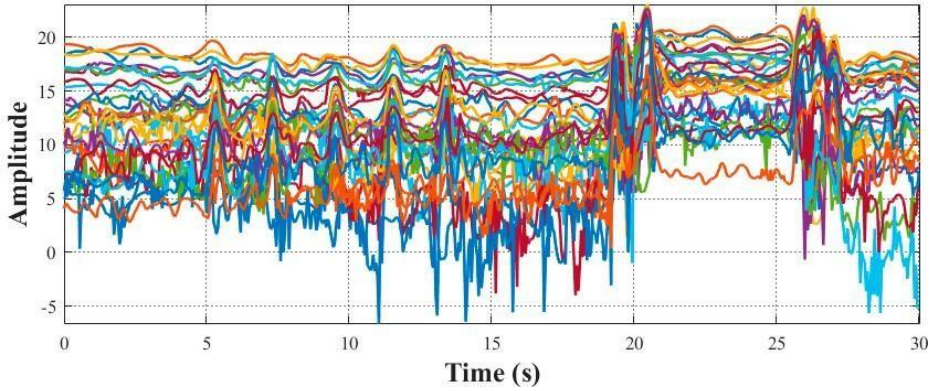

Figure 7. Wavelet-filtered CSI signals.

2.3.3. Moving Average Filter

For the CSI signals after wavelet filtering, we employed a moving average filter to further smooth the signals, reducing the influence of high-frequency noise and preserving the trend of signals in the time domain. Briefly, given a signal sequence x_n containing N samples, where n is the index of the sample, moving average filtering was performed by sliding a window of fixed length M over the signal sequence and computing the mean of the samples within the window. For each position k of the sliding window, the filtered output y_k can be calculated using the following equation:

$$y = \frac{x_k + x_{k-1} + x_{k-2} + \cdots + x_{k-M+1}}{M} \quad (5)$$

During data processing, we set the length of the sliding window M to 20, which is the same as the value of the packet transmission rate. Figure 8 shows the CSI signals after applying the moving average filter. Compared to Figure 7, we can clearly see that the high-frequency noise is further suppressed, and the trends of CSI signals induced by human activities (i.e., walking 5 times, jumping 1 time, and falling 1 time) are much clearer and neater. Figure 9 shows a comparison of the changes in CSI signals before and after filtering. We can clearly see that, compared to the raw CSI signals, the filtered CSI signals become neater and the trend of recorded human activity changes is more obvious.

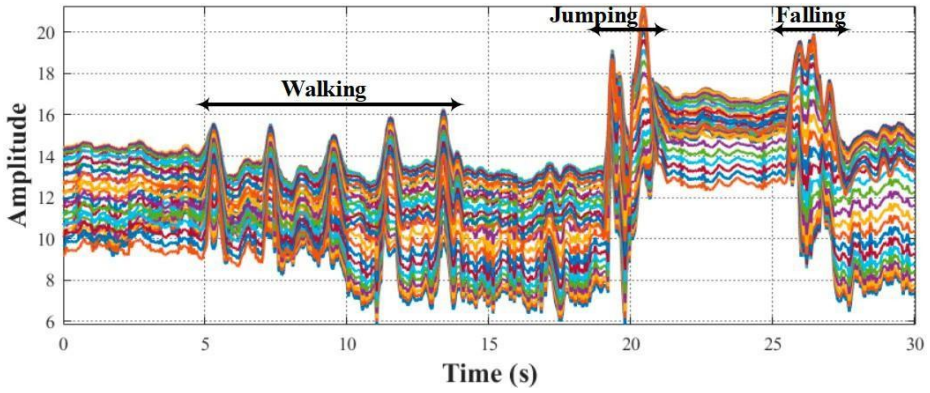

Figure 8. CSI signals after applying moving average filter.

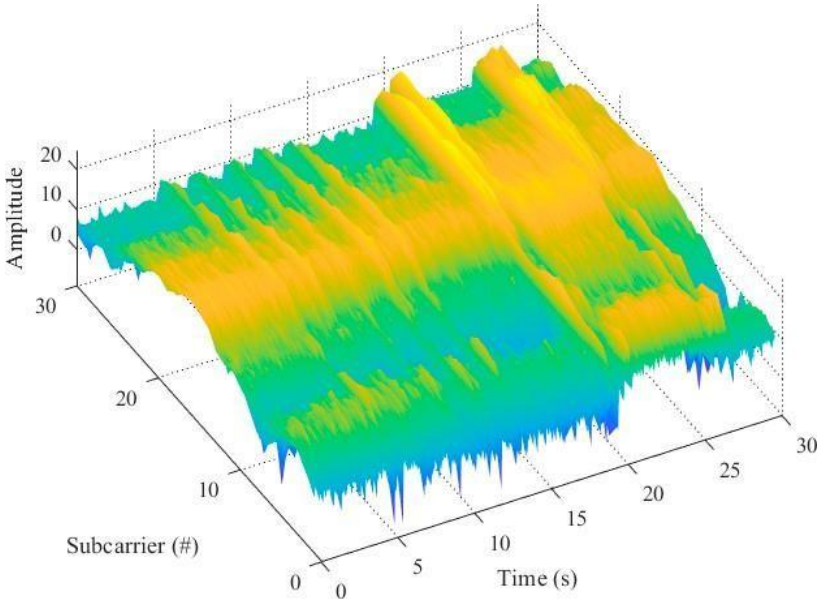

(**a**)

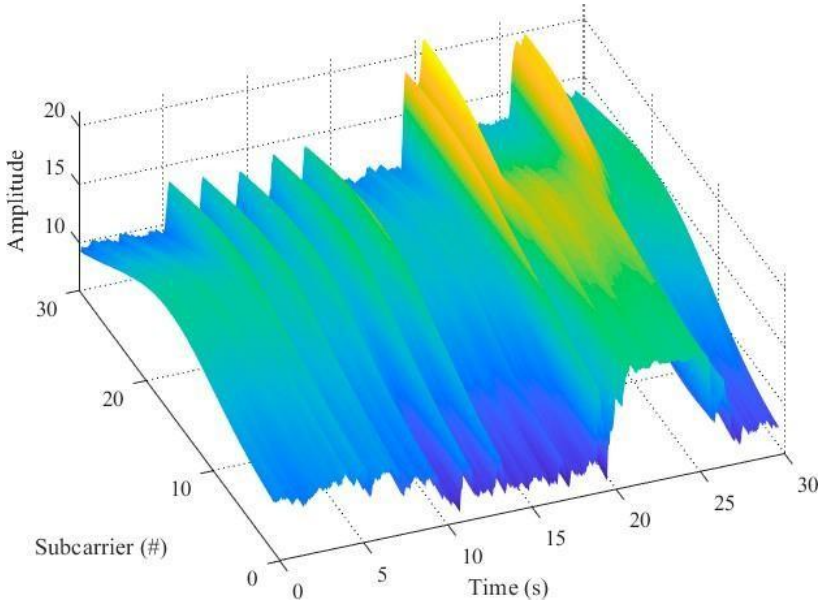

(**b**)

Figure 9. CSI signal changes under human activity. (**a**) Raw CSI signals. (**b**) Filtered CSI signals.

2.3.4. Carrier Selection

As different subcarriers have different center frequencies/wavelengths, this leads to varying sensitivities of different subcarriers to human activities. As shown in Figure 9b, we can roughly see that subcarriers 25–30 could better perceive the changes in CSI amplitude caused by human activities, while subcarriers 1–15 had lower sensitivity to changes in human activities. Therefore, it is crucial to select an optimal set of subcarriers from the 30 candidate subcarriers that can fully record the changes in human activities. From Figure 8, it is easy to see that for any human activity-induced change in the CSI signal segment, its shape in the time domain is like a 'mountain peak.' Therefore, an ideal subcarrier should be able to fully depict the set of 'peaks' caused by human activities. Based on this observation, we define a new metric for selecting an optimal set of subcarriers, whichis computed based on two statistics: kurtosis and standard deviation. Specifically, given

any segment of the CSI amplitude sequence $C^i = \{c^i, \ldots, c^i\}$, where i is the subcarrier sequence number and n is the number of sample points, the sensitivity of $C^i = \{c^i, \ldots, c^i\}$ to human activity can be expressed as

$$Q_{(1,n)}^i = (1-\theta) \times sd^i + \theta \times kt^i \quad (6)$$

$$sd^i = \sqrt{\frac{\sum_{j=1}^{n} (c_j^i - \underline{c})^2}{n}} \quad (7)$$

$$kt^i = \frac{\frac{1}{n}\sum_{j=1}^{n} (c_j^i - \underline{c})^4}{\left(\frac{1}{n}\sum_{j=1}^{n} (c_j^i - \underline{c})^2\right)^2} - 3 \quad (8)$$

where sd^i and kt^i are the standard deviation and kurtosis of C^i, respectively, and $\theta \in [0, 1]$ is the weighting factor. We empirically set θ to 0.6.

The sensitivity values of all 30 subcarriers to human activities were calculated accord- ing to Equation (6), as shown in Figure 10. We can observe that the different subcarriers have different sensitivities to human activity, where subcarriers 16–19 present small sensi- tivity values (less than 2), while subcarriers 26–30 have relatively high sensitivity values (greater than 3.5). The sensitivities of subcarriers 18 and 30 presented the minimum and maximum values, respectively. When comparing Figures 9b and 10, we can see that the subcarrier sensitivity calculated based on the proposed metric can better reveal the ampli- tude changes in CSI caused by human activities. Figure 11 shows the changes in human activities recorded by subcarrier 30. Overall, the results indicate that the proposed metric achieves effectiveness in selecting the optimal subcarrier set.

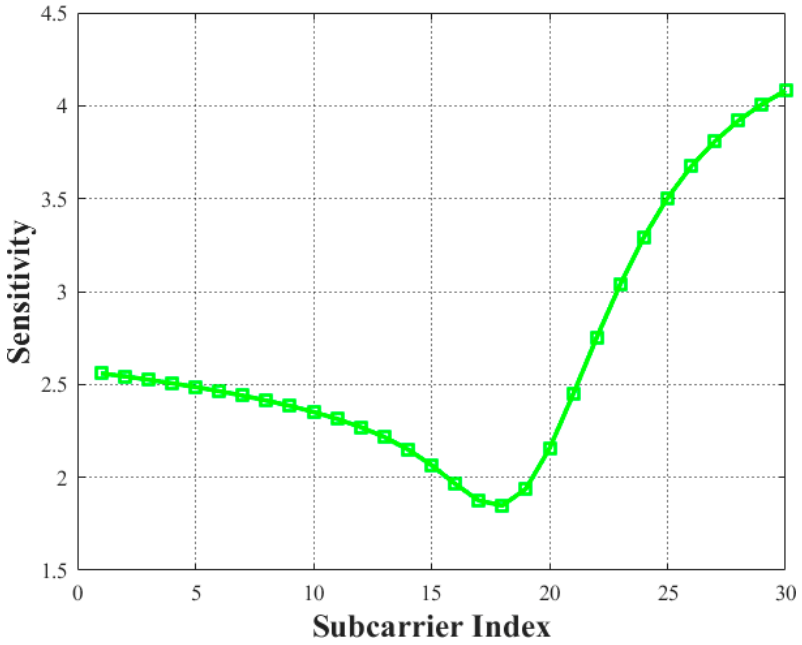

Figure 10. Calculated sensitivity of each subcarrier to human activity.

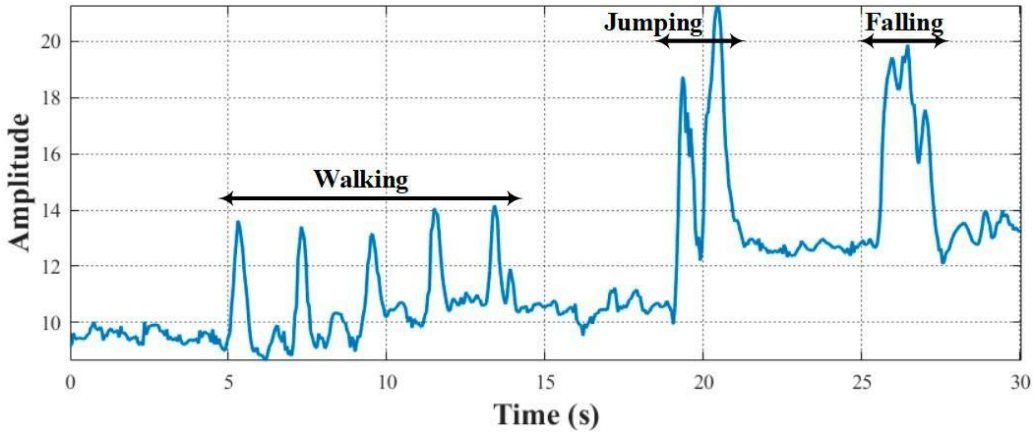

Figure 11. CSI amplitude under different human activities (subcarrier 30).

2.4. *Motion Recognition*

After obtaining the sensitivity values of all 30 subcarriers, we selected the top-ten subcarriers according to their sensitivity values in order to construct an optimal set of subcarriers. Then, we segmented the 10 subcarriers in the set and extracted a set of effectivefeature sets to train an SVM model. Finally, the trained classification model was utilized to achieve non-invasive, low-cost, and accurate human activity detection.

2.4.1. Data Segments

In order to accurately segment the CSI segments that completely record a particular human activity from a continuous CSI signal, we set up a window as a unit to extract features. The duration of the window should be neither too long nor too short, given that a long window time can introduce irrelevant target actions, while a short window timecan lead to incomplete target actions. As the duration of a single target human action(i.e., walking, jumping, or falling) usually does not exceed 3 s, we set the duration of the window to that value. Specifically, we first used the classical peak-finding algorithm to find a set of data points with local maxima from the CSI signal, and then segmented the CSI segments with a duration of 3 s from the CSI signal using the data points as the midpoints. Finally, we performed feature extraction on the segmented CSI segments to train the classification model.

2.4.2. Feature Extraction and Classification

From Figure 11, it can be seen that walking induces smaller fluctuations in CSI ampli- tude and a shorter duration of the movement compared to jumping and falling. Meanwhile, compared to the smoother and more continuous falling action, the jumping action can usually be decomposed into several consecutive sub-movements. Based on observationsof the data and referring to the work of Liu et al. [31], we extracted a set of feature sets containing both time- and frequency-domain features (as shown in Table 1) in order to better train the classification model. Although deep neural networks (DNNs) and convolu- tional neural networks (CNNs) have shown strong capabilities in feature extraction recently, they typically require a large number of training samples and have strict requirements on hardware operating parameters. Considering the multiple overheads (e.g., time, money, human resources) of performing the data collection and model training tasks, we could only collect a limited number of training samples with affordable overheads in our work and, so, we trained the classifier model using a lightweight machine learning algorithm, namely, SVM.

Table 1. Features used in our system.

Time-Domain Features
max, min, mean, variance, standard deviation, max–min, kurtosis, skewness, mean crossing rate
Frequency-Domain Features
energy, frequency, sensitivity

3. Evaluation

In this section, we first introduce the system implementation, then evaluate the overall performance of the proposed system; finally, we further discuss the impact of different influencing factors on system performance.

3.1. Implementation

3.1.1. Hardware and Software Implementation

Figure 4 shows the hardware deployment of the system. We used a TP Link WDR5620 wireless router (TP-Link Technology Co., Ltd., Shenzhen, Guangdong Province, China) as the transmitter of the system, with its operating frequency set to 2.4 GHz, and used a Lenovo desktop computer (Lenovo Group, Beijing, China) with a built-in Intel 5300 network card as the receiver. The transmitter and receiver were both placed on the desk, with a relative distance of about 2 m. We set the transmission rate to 20 pkts/s. In addition, to enhance the strength of the received signal, we attached three antennas with a gain of 6 dBi to the network card of the receiver. Note that we also utilized the HD surveillance device already installed in the office to capture video data recording indoor human activities in order to obtain the ground truth and label the dataset. We applied a tool provided in the literature [36] to obtain CSI measurements of the 30 subcarriers from the network card of the receiver. We directly processed and analyzed the collected CSI measurement values on a Lenovo desktop computer running Ubuntu 16.04 LTS, and used Matlab 2018b to write programs to implement the functions in the data processing and motion analysis shown in Figure 3.

3.1.2. Environment and Participants

To evaluate the performance of the proposed system, we invited 10 volunteers to participate in the experiment in the office shown in Figure 4. The 10 volunteers included four children (two boys and two girls) and six adults (three males and three females), who had a height range of 145 cm to 180 cm and a weight range of 30 kg to 80 kg. During the one-month experiment, we asked each of the volunteers to perform human activities including walking (30 times), jumping (30 times), and falling (30 times) on a foam mat every day. Therefore, we captured a total of 270,000 CSI data segments (30 times $\times$ 10 subcarriers $\times$ 30 days $\times$ 3 types of human activities $\times$ 10 people). Note that all experiments were approved by our Institutional Review Board.

3.1.3. Performance Metrics

To quantify the recognition performance of the classifier model on human activities, we used three evaluation metrics: accuracy, F1 score, and confusion matrix. These metrics are calculated as follows:

$$\text{accuracy} = \frac{TP + TN}{TP + FP + TN + FN} \times 100\% \quad (9)$$

where TP, TN, FP, and FN represent true positive, true negative, false positive, and false negative, respectively.

$$\text{F1 score} = \frac{2 \times \text{Precision} \times \text{Recall}}{\text{Precision} + \text{Recall}} \times 100\% \quad (10)$$

where Precision $= \frac{TP}{TP+FP}$ and Recall $= \frac{TP}{TP+FN}$. For the confusion matrix, each of its columns represents the predicted activity while each row represents the real activity.

3.2. *Overall Performance*

The recognition performance of the proposed system for indoor human activities, including walking, jumping, and falling, is shown in Figure 12. We can observe that the system recognized walking, jumping, and falling with an accuracy of 100%, 90%, and 97%, respectively. This result is basically consistent with the phenomenon shown in Figure 8. Compared to jumping and falling, walking caused significantly smaller changes in CSI amplitude. As a result, while the system could accurately recognize walking, there were still some errors in distinguishing between jumping and falling. Overall, the proposed system obtained an average accuracy of more than 95% in recognizing walking, jumping, and falling. Figure 12 further illustrates the recognition performance of the system for different volunteers. In the figure, we use symbols 'M', 'W', 'G', and 'B' to represent adult males, adult females, girls, and boys, respectively. The detection performance of the system for adults and children (i.e., accuracy and F1 score) was approximately 95% and 90%, respectively. The main reason for this result is that, compared to adults, children's activities cause weaker fluctuations in CSI amplitude due to their lower limb movement speeds and amplitudes. Weaker CSI amplitude fluctuations increase the challenge for classifiers in recognizing different activities. Furthermore, we can see, from Figure 13, that there was no correlation between the detection performance of the system and the gender of the user.

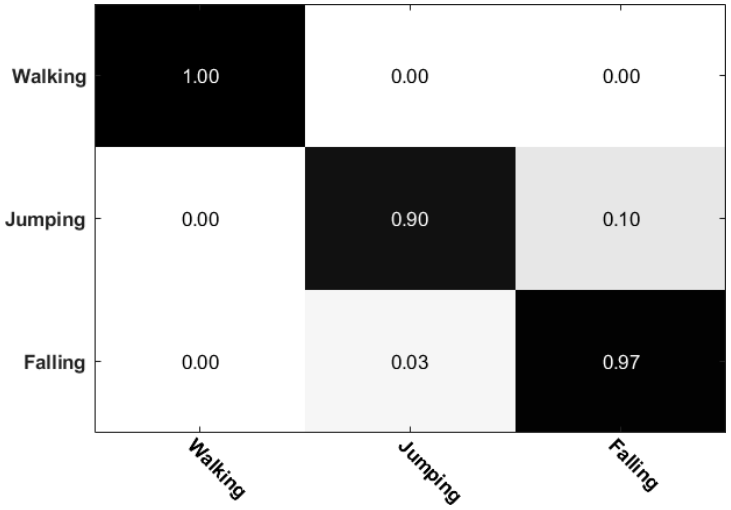

Figure 12. The overall performance of the proposed system.

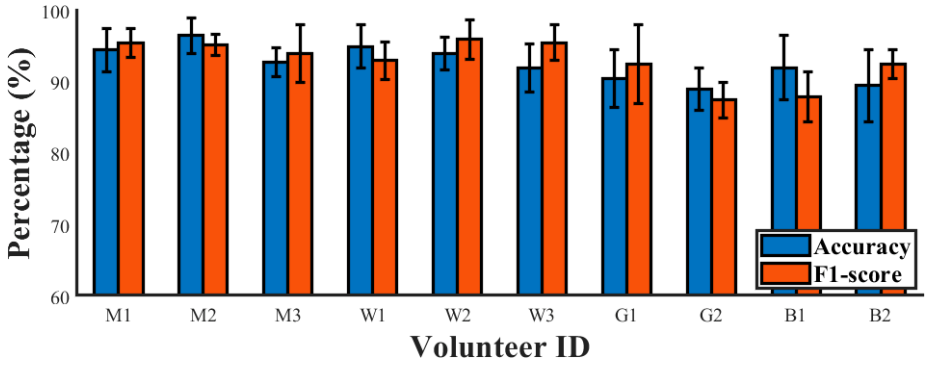

Figure 13. The recognition performance of the system for different users.

3.3. *Impacts of Different Factors*

As shown in Figure 4, we can speculate that the distance between transceivers and their height from the ground may affect the performance of the system. In this section, we further discuss the impact of these factors on the robustness of the system.

3.3.1. Impact of Transceiver Distance

We first investigated the impact of the relative distance between transceivers on the detection performance of the system. The distance between the transmitter and receiverwas increased from 2 m to 3.5 m at an interval of 0.5 m. Then, we randomly invited 4 of the 10 volunteers to participate in the experiment. Figure 14 shows the system detectionperformance at different transceiver distances. When the distance between the transceivers was set to 2 m, 2.5 m, 3 m, and 3.5 m, the average accuracy and F1 score of the proposed system for detecting human activity both remained higher than 93%. We can see that the performance of the proposed indoor human activity monitoring system decreased slightly with a gradual increase in transceiver distance. The main reason for this result is that thestrength of the received signal decreases due to the growth of communication distance, leading to smaller CSI amplitude fluctuations. Overall, as long as the distance between the transceivers is less than 3.5 m, the system can still achieve an acceptable detection performance (average accuracy and F1 score above 93%).

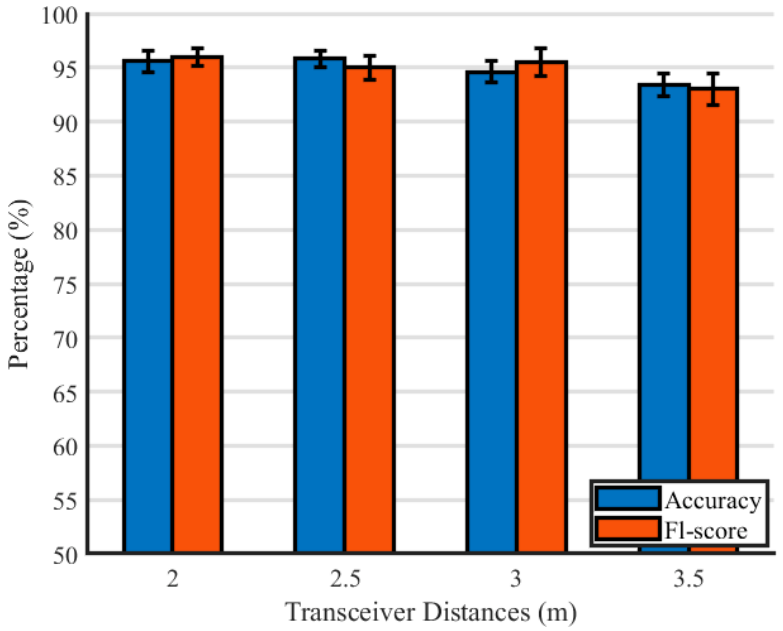

Figure 14. The impact of transceiver distance.

3.3.2. Impact of Transceiver Height

We then investigated the effect of the height of the transceiver from the ground on the detection performance of the system. The height of the transceiver from the ground was increased from 0.75 m to 1.35 m at an interval of 0.2 m. We also randomly invited 4 of the 10 volunteers to participate in this experiment. Figure 15 shows the detection performance of the system at different transceiver heights, from which it can be observed that the proposed system achieves an average accuracy and F1 score of about 95% for human activitydetection under different transceiver height conditions. Overall, the detection performance of the proposed system is almost insensitive to the adjustment of transceiver height.

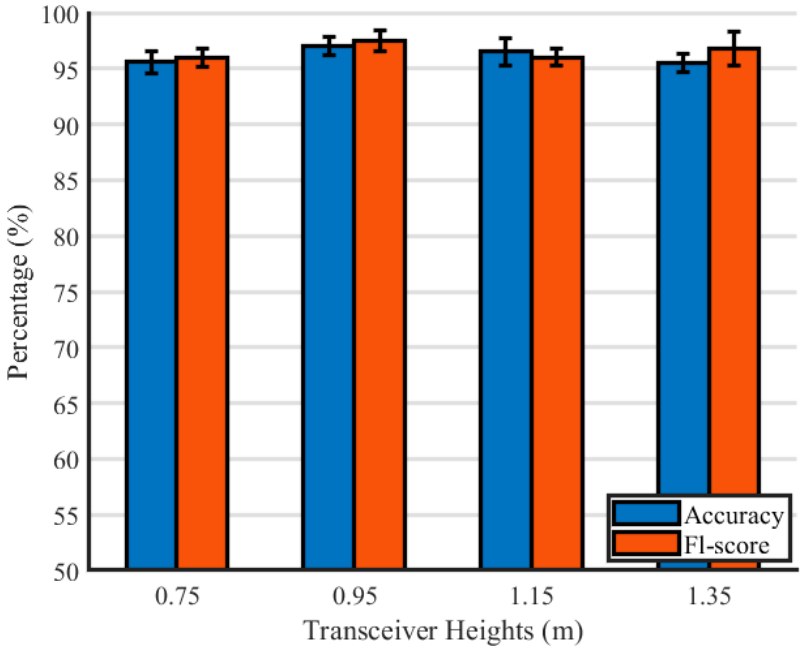

Figure 15. The impact of transceiver height.

3.3.3. Impact of Different Classifiers

We further explored the recognition performance of the proposed system under three other classification models, including random forest (RF), k nearest neighbors (k-NN), and decision tree (DT). We evaluated the performance of each classifier using 10 -fold cross-validation. For each cross-validation, we ensured that the training/testing datasets between different classifiers were the same. The results for the recognition performance of different classifiers on target human activities are shown in Table 2. We can clearly observe that the average recognition accuracy of the four classifiers for human activities is 95.7%, 92.8%, 91.6%, and 94.3%, respectively. The accuracy of the SVM model is over 95%, which isslightly better than the other three classifiers. Note that by fine-tuning parameters or using more training data, we can further improve the performance of other classifiers. Overall, the proposed system can achieve a satisfactory recognition performance (accuracy above 90%) under different classifiers.

Table 2. Performance comparison of different classifiers.

	Classifier			
Metric (%)	**SVM**	**k-NN**	**DT**	**RF**
Accuracy	95.7	92.8	91.6	94.3
F1-score	96	92.3	92.1	94.8

4. Discussion

Although the proposed system is capable of achieving contactless, low-cost, and secure indoor human activity detection through use of the existing ubiquitous WiFi signals, its limitations are also clear when compared with most of the existing related works. For example:

- Subtle movement. The proposed system only uses a low-cost COTS router as a trans- mitter, which limits its ability to sense subtle movements (e.g., heartbeat, respiration, and cough). We will try to deploy a high-gain directional antenna to enhance the
power of the transmitted signal or some wearable and skin-attachable sensors to collectmore fine-grained information in future experiments so that the proposed method can provide a higher sensing accuracy in recognizing human activity.

- Multiple users. The proposed system can only be applied to sense one person's body movements at a time. The receiver will collect a mixed signal recording multiple users' body movements if they perform activities simultaneously, and it is challenging to
  decouple the CSI signals of individual body movements from the mixed signal.
- Cross-domain. The performance of the proposed system relies on environment-related domains including position, orientation, and static objects. As such, a classifier model
  trained using data collected in a given environment may not perform well in a new environment. We will try to apply transfer learning or adversarial learning method-ologies to improve the cross-domain sensing performance in future work.

5. Conclusions

In this study, the existing ubiquitous radio frequency signals generated by a COTS WiFi router were utilized to recognize indoor human activities, including walking, jumping, and falling, providing an approach that is non-intrusive, low-cost, and secure for users. In order to achieve accurate and robust detection, we first applied multiple filters to eliminate the outliers and ambient noise existing in original CSI measurements, to obtain fine-grained CSI signals. Then, an optimal set of subcarriers sensitive to all target activities was selected based on a novel metric, and we finally extracted a set of effective features to train an SVM-based activity recognition system. Extensive experiments involving 10 participants were conducted, and the results demonstrated that the proposed system achieved 95% accuracy in recognizing walking, jumping, and falling activities. We envision that the proposed method can be utilized in various indoor applications, thus benefiting people in their daily lives.

or financial relationships that could be construed as a potential conflict of interest.

References

1. Kushida, C.A.; Littner, M.R.; Morgenthaler, T.; Alessi, C.A.; Bailey, D.; Coleman, J., Jr.; Friedman, L.; Hirshkowitz, M.; Kapen, S.; Kramer, M.; et al. Practice parameters for the indications for polysomnography and related procedures: An update for 2005. *Sleep* **2005**, *28*, 499–523. [CrossRef] [PubMed]
2. Aurora, R.N.; Zak, R.S.; Karippot, A.; Lamm, C.I.; Morgenthaler, T.I.; Auerbach, S.H.; Bista, S.R.; Casey, K.R.; Chowdhuri, S.; Kristo, D.A.; et al. Practice parameters for the respiratory indications for polysomnography in children. *Sleep* **2011**, *34*, 379–388. [CrossRef]
3. Zhang, S.; McCullagh, P.; Zhang, J.; Yu, T. A smartphone based real-time daily activity monitoring system. *Clust. Comput.* **2014**, *17*, 711–721. [CrossRef]
4. Qi, W.; Su, H.; Aliverti, A. A smartphone-based adaptive recognition and real-time monitoring system for human activities. *IEEE Trans. Hum.-Mach. Syst.* **2020**, *50*, 414–423. [CrossRef]
5. Ramanujam, E.; Perumal, T.; Padmavathi, S. Human activity recognition with smartphone and wearable sensors using deep learning techniques: A review. *IEEE Sens. J.* **2021**, *21*, 13029–13040. [CrossRef]
6. Zhuang, Z.; Xue, Y. Sport-related human activity detection and recognition using a smartwatch. *Sensors* **2019**, *19*, 5001. [CrossRef]
7. Ashry, S.; Ogawa, T.; Gomaa, W. CHARM-deep: Continuous human activity recognition model based on deep neural network using IMU sensors of smartwatch. *IEEE Sens. J.* **2020**, *20*, 8757–8770. [CrossRef]
8. Boyer, P.; Burns, D.; Whyne, C. Out-of-distribution detection of human activity recognition with smartwatch inertial sensors. *Sensors* **2021**, *21*, 1669. [CrossRef]
9. Jahan, I.; Al-Nabhan, N.A.; Noor, J.; Rahaman, M.; Al Islam, A.A. Leveraging A Smartwatch for Activity Recognition in Salat. *IEEE Access* **2023**, *11*, 97284–97317. [CrossRef]
10. Fang, B.; Lane, N.D.; Zhang, M.; Boran, A.; Kawsar, F. BodyScan: Enabling radio-based sensing on wearable devices for contactless activity and vital sign monitoring. In Proceedings of the 14th Annual International Conference on Mobile Systems, Applications, and Services, Singapore, 26–30 June 2016; pp. 97–110.
11. Fang, B.; Lane, N.D.; Zhang, M.; Kawsar, F. Headscan: A wearable system for radio-based sensing of head and mouth-related activities. In Proceedings of the 2016 15th ACM/IEEE International Conference on Information Processing in Sensor Networks (IPSN), Vienna, Austria, 11–14 April 2016; pp. 1–12.
12. Wang, T.; Zhang, D.; Wang, L.; Zheng, Y.; Gu, T.; Dorizzi, B.; Zhou, X. Contactless respiration monitoring using ultrasound signal with off-the-shelf audio devices. *IEEE Internet Things J.* **2018**, *6*, 2959–2973. [CrossRef]
13. Chen, Y.; Gong, W.; Liu, J.; Cui, Y. I can hear more: Pushing the limit of ultrasound sensing on off-the-shelf mobile devices. In Proceedings of the IEEE INFOCOM 2018-IEEE Conference on Computer Communications, Honolulu, HI, USA, 16–19 April 2018; pp. 2015–2023.
14. Zhai, S.; Ye, G.; Tang, Z.; Ren, J.; Fang, D.; Liu, B.; Wang, Z. Towards practical 3D ultrasound sensing on commercial-off-the-shelf mobile devices. *Comput. Netw.* **2021**, *191*, 107990. [CrossRef]
15. Zhang, S.; Wei, Z.; Nie, J.; Huang, L.; Wang, S.; Li, Z. A review on human activity recognition using vision-based method. *J. Healthc. Eng.* **2017**, *2017*, 3090343. [CrossRef]
16. Beddiar, D.R.; Nini, B.; Sabokrou, M.; Hadid, A. Vision-based human activity recognition: A survey. *Multimed. Tools Appl.* **2020**, *79*, 30509–30555. [CrossRef]
17. Qi, W.; Wang, N.; Su, H.; Aliverti, A. DCNN based human activity recognition framework with depth vision guiding. *Neurocom- puting*

2022, *486*, 261–271. [CrossRef]
18. Wang, X.; Wu, Z.; Jiang, B.; Bao, Z.; Zhu, L.; Li, G.; Wang, Y.; Tian, Y. Hardvs: Revisiting human activity recognition with dynamicvision sensors. In Proceedings of the AAAI Conference on Artificial Intelligence, Vancouver, BC, Canada, 20–28 February 2024; Volume 38, pp. 5615–5623.
19. Gu, F.; Chung, M.H.; Chignell, M.; Valaee, S.; Zhou, B.; Liu, X. A survey on deep learning for human activity recognition. *ACM Comput. Surv. (CSUR)* **2021**, *54*, 1–34. [CrossRef]
20. Li, X.; He, Y.; Jing, X. A survey of deep learning-based human activity recognition in radar. *Remote Sens.* **2019**, *11*, 1068. [CrossRef]
21. Li, X.; He, Y.; Fioranelli, F.; Jing, X. Semisupervised human activity recognition with radar micro-Doppler signatures. *IEEE Trans. Geosci. Remote Sens.* **2021**, *60*, 1–12. [CrossRef]
22. Cao, Z.; Li, Z.; Guo, X.; Wang, G. Towards cross-environment human activity recognition based on radar without source data. *IEEE Trans. Veh. Technol.* **2021**, *70*, 11843–11854. [CrossRef]
23. Yu, C.; Xu, Z.; Yan, K.; Chien, Y.R.; Fang, S.H.; Wu, H.C. Noninvasive human activity recognition using millimeter-wave radar. *IEEE Syst. J.* **2022**, *16*, 3036–3047. [CrossRef]
24. Alhazmi, A.K.; Alanazi, M.A.; Alshehry, A.H.; Alshahry, S.M.; Jaszek, J.; Djukic, C.; Brown, A.; Jackson, K.; Chodavarapu, V.P. Intelligent Millimeter-Wave System for Human Activity Monitoring for Telemedicine. *Sensors* **2024**, *24*, 268. [CrossRef]
25. Huang, T.; Liu, G.; Li, S.; Liu, J. RPCRS: Human Activity Recognition Using Millimeter Wave Radar. In Proceedings of the 2022 IEEE 28th International Conference on Parallel and Distributed Systems (ICPADS), Nanjing, China, 10–12 January 2023; pp. 122–129.
26. Yin, W.; Shi, L.F.; Shi, Y. Indoor human action recognition based on millimeter-wave radar micro-doppler signature. *Measurement* **2024**, *235*, 114939. [CrossRef]
27. Khan, M.B.; Yang, X.; Ren, A.; Al-Hababi, M.A.M.; Zhao, N.; Guan, L.; Fan, D.; Shah, S.A. Design of software defined radios based platform for activity recognition. *IEEE Access* **2019**, *7*, 31083–31088. [CrossRef]
28. Ashleibta, A.M.; Zahid, A.; Shah, S.A.; Abbasi, Q.H.; Imran, M.A. Flexible and scalable software defined radio based testbed for large scale body movement. *Electronics* **2020**, *9*, 1354. [CrossRef]
29. Saeed, U.; Shah, S.A.; Khan, M.Z.; Alotaibi, A.A.; Althobaiti, T.; Ramzan, N.; Imran, M.A.; Abbasi, Q.H. Software-defined radio based contactless localization for diverse human activity recognition. *IEEE Sens. J.* **2023**, *23*, 12041–12048. [CrossRef]
30. Wang, Y.; Zheng, Y. Modeling RFID signal reflection for contact-free activity recognition. *Proc. ACM Interact. Mob. Wearable Ubiquitous Technol.* **2018**, *2*, 1–22. [CrossRef]
31. Liu, C.; Xiong, J.; Cai, L.; Feng, L.; Chen, X.; Fang, D. Beyond respiration: Contactless sleep sound-activity recognition using RFsignals. *Proc. ACM Interact. Mob. Wearable Ubiquitous Technol.* **2019**, *3*, 1–22. [CrossRef]
32. He, X.; Zhu, J.; Su, W.; Tentzeris, M.M. RFID based non-contact human activity detection exploiting cross polarization. *IEEE Access* **2020**, *8*, 46585–46595. [CrossRef]
33. Wang, F.; Liu, J.; Gong, W. Multi-adversarial in-car activity recognition using RFIDs. *IEEE Trans. Mob. Comput.* **2020**, *20*, 2224–2237. [CrossRef]
34. Colella, R.; Tumolo, M.R.; Sabina, S.; Leo, C.G.; Mincarone, P.; Guarino, R.; Catarinucci, L. Design of UHF RFID sensor-tags forthe biomechanical analysis of human body movements. *IEEE Sens. J.* **2021**, *21*, 14090–14098. [CrossRef]
35. Guo, X.; Liu, J.; Shi, C.; Liu, H.; Chen, Y.; Chuah, M.C. Device-free Personalized Fitness Assistant Using WiFi. *Proc. ACM Interact.Mob. Wearable Ubiquitous Technol.* **2018**, *2*, 1–23. [CrossRef]
36. Halperin, D.; Hu, W.; Sheth, A.; Wetherall, D. Tool release: Gathering 802.11 n traces with channel state information. *ACM SIGCOMM Comput. Commun. Rev.* **2011**, *41*, 53. [CrossRef]